Improved Cellular Uptake of Perfluorocarbon Nanoparticles for In Vivo Murine Cardiac ^{19}F MRS/MRI and Temporal Tracking of Progenitor Cells

Christakis Constantinides[a*], Ph.D., Eileen McNeill[a], Ph.D., Ricardo Carnicer[a], Ph.D., Ayman Al Haj Zen [a], M.D., Ph.D., Raquel Sainz Urruela[b,c], Ph.D., Andrew Shaw[a], Ph.D., Jyoti Patel[a], Ph.D., Edyta Swider[e], M.S., Rita Alonaizan[d], B.S., Louiza Potamiti[f], M.Sc., Andreas Hadjisavvas[f], Ph.D., Sergi Padilla-Parra[b,c], Ph.D., Kyriacos Kyriacou[f], Ph.D., Mangala Srinivas[e†], Ph.D., Carolyn A. Carr[d†], Ph.D.

Submitted as an Original Research Article

Correspondence Address: Dr. C. Constantinides

[a]Radcliffe Department of Medicine

Department of Cardiovascular Medicine

Wellcome Trust Centre for Human Genetics

[b]Division of Structural Biology

University of Oxford

Henry Wellcome Building for Genomic Medicine

Headington

Oxford OX3 7BN

UK

[c]Wellcome Trust Centre for Human Genetics

Cellular Imaging Core

University of Oxford

Oxford OX3 7BN

[d]Department of Physiology, Anatomy, and Genetics

University of Oxford

South Parks Road

Oxford OX13QX

UK

[e]Radboud University Medical Center (RadboudUMC)

Department of Tumor Immunology, 278

Radboud Institute for Molecular Life Sciences (RIMLS)

Postbox 9101

6500HB Nijmegen

The Netherlands

[f]Department of Electron Microscopy/Molecular Pathology

The Cyprus Institute of Neurology and Genetics and The Cyprus School of Molecular Medicine

6 International Airport Avenue

2370 Nicosia

Cyprus

Competing Interests: None

Abstract Word Count: 150 words

Word Count: 4694 words (body text and figure/table legends)

Number of References: 35

Number of Figures: 8

Supplementary Figures: ~~4~~

Number of Online Figures: ~~4~~ (for Supplementary Figure 1)

Number of Tables: 1

Funding: The project was supported by the European Union's Horizon 2020 research and innovation programme under the Marie Sklodowska-Curie [grant agreement No. 652986 (CC)], the European Research Council [grant ERC-2013-StG-336454 (MS)], and from the BHF Centre of Regenerative Medicine, Oxford, and the BHF Centre of Research Excellence, Oxford (CAC).

Disclosure Statement: Dr. C. Constantinides has been a co-director of Chi-Biomedical Ltd. (Cyprus) since 2005. Chi-Biomedical has been in a financial dormant status during the past 5 years. There are no conflicts of interest to disclose.

*Corresponding author

Present address:

Chi Biomedical Ltd.

2 Evryviadou Street

Mezzanie Apartment 1

Limassol 4150

Cyprus

Tel: (Cyprus) +35796711475/+35722345839

Email: Christakis.Constantinides@gmail.com

†These authors contributed equally to this work

Abstract

Herein, we maximize the labeling efficiency of cardiac progenitor cells (CPCs) using perfluorocarbon nanoparticles (PFCE-NP) and ^{19}F MRI detectability, determine the temporal dynamics of single-cell label uptake, quantify the temporal viability/fluorescence persistence of labeled CPCs in vitro, and implement in vivo, murine cardiac CPC MRI/tracking that could be translatable to humans.

FuGENE^{HD}-mediated CPC PFCE-NP uptake is confirmed with flow cytometry/confocal microscopy. Epifluorescence imaging assessed temporal viability/fluorescence (up to 7 days [D]). Nonlocalized murine ^{19}F MRS and cardiac MRI studied label localization in terminal/longitudinal tracking studies at 9.4T (D1–D8).

A 4–8 fold ^{19}F concentration increase is evidenced in CPCs for FuGENE vs. directly labeled cells. Cardiac ^{19}F signals post-CPC injections diminished in vivo to ~31% of their values on D1 by D7/D8. Histology confirmed CPC retention, dispersion, and macrophage-induced infiltration. Intra-cardiac injections of PFCE-NP-labeled CPCs with FuGENE can be visualized/tracked in vivo for the first time with ^{19}F MRI.

Keywords: Fluorine MRI, perfluorocarbon nanoparticles, cardiac stem cells, macrophages, tracking.

(Graphical Abstract: Modified Figure 7)

1. Introduction

Implantation of stem cells (SCs)[1] promises cardiac tissue regeneration and structural and functional improvements following injury [1]. While the feasibility of SC therapies has been proven, efficacy has yet to be demonstrated conclusively [2].

In recent years, perfluorocarbon nanoparticles (PFCE-NPs) have been applied in numerous therapeutic applications [3] and have led to direct tracking and quantification of labeled SCs and other cell populations using ^{19}F-MRI [4–8], benefitting from fluorine's MR visibility, the lack of in vivo tissue/organ content, and clinical relevance. However, to-this-date, there are significant challenges and limitations with this approach [9], such as the efficiency of label uptake, compromizing cellular fate and cardiac signal detectability in vivo [2].

Different agents commonly used for DNA transfection (FuGENE^{HD}, lipofectamine, others), herein referred to as "labeling agents", have been employed [10–14] to increase the efficiency of cellular uptake of ^{19}F compounds, targeting immune-based therapies [6, 7, 15], and work unrelated to the direct administration of cardiac SCs [16, 17, 18]. Alternative strategies using

[1] ANOVA: Analysis of variance; BW: Bandwidth; CPCs: Cardiac progenitor cells; CDCs: Cardiosphere-derived cells; CT: Collagenase/Trypsin; DAPI: 4',6-diamidino-2-phenylindole; ECG: Electrocardiographic; FLASH: Fast low-angle shot; FOV: Field-of-view; FSC: Forward scatter; GFP: Green fluorescent protein; IMDM: Iscove's Modified Dulbecco's Medium; ISO: Isoflurane; LV: Left-ventricular; MPIOs: Iron oxide particles; MRI: Magnetic Resonance Imaging; MRS: Magnetic Resonance Spectroscopy; NPs: Nanoparticles; NEX: Number of excitations; PFCE-NPs: Perfluoro-crown-ether nanoparticles; PFCE: Perfluoro-crown-ethers; PBS: Phosphate buffer solution; PW: Pulse width; RF: Radiofrequency; SSC: Side scatter; SCs: Stem cells; SNR: Signal-to-noise-ratios; SPIO: Superparamagnetic iron oxide; ST: Slice thickness; SPGR: Spoiled gradient echo; TE: Echo time; TR: Repetition time; TFA: Trifluoroacetic acid; 2D: Two-dimensional; 3D: Three-dimensional.

electroporation techniques have led to moderate label payload increases (^{19}F or other) [19, 20, 21, 18] at the expense of increased risks of cellular toxicity, difficulties in optimization, imbalances of cell homeostasis, and possible permanent permeabilization of the plasma membrane [21, 18].

Despite prior ^{19}F MRI advances in the visualization of pre-labeled SCs with PFCE-NPs or other MRI contrast agents [5, 15], there have been no prior reports on murine cardiac ^{19}F imaging of exogenously administered cardiac SCs following direct, intra-cardiac injections. To-this-date, human or in vivo murine studies are lacking, while prior reported imaging attempts in rats have been prohibitively lengthy, costly (multiple millions of cells/animal), and practically complex to reproduce in mice [20, 22].

Invariably, low-label uptake is prohibitive for the visualization and tracking of labeled SCs in longitudinal cardiac applications in vivo.

In this proof-of-principle study, we show significant enhancements of PFCE-NP label uptake in two types of cardiac progenitor cells (CPCs) [23] following labeling with the agent FuGENE [24], thereby accomplishing in vivo cardiac ^{19}F MRI visualization and tracking with minimal cellular toxicity. We report significant improvements of ^{19}F MRI signal detection in the labeled CPCs (cardiosphere-derived (CDCs) and collagenase-trypsin (CT) cells) using FuGENE compared to directly labeled or electroporated cells. CDCs have been shown to improve cardiac function in models of MI, whereby administered cells were retained—albeit in low numbers—and expressed cardiac proteins [23, 26, 27]. CT cells have been isolated by enzymatic digestion and slow adhesion and have a comparable gene expression and differentiation profile to CDCs [28].

The purposes of the study are to a) maximize the labeling efficiency of CPCs using PFCE-NPs and the ^{19}F MRI detectability, b) determine the temporal dynamics of single-cell label uptake, c) quantify the temporal viability/fluorescence persistence of labeled CPCs in vitro, and d) implement an in vivo, murine cardiac CPC administration protocol, ^{19}F MRI and tracking, that could be translatable to human applications.

2. Methods

Animal Ethics

All experimental procedures in this prospective, proof-of-principle animal study were approved by the Home Office, UK and International regulatory bodies, and adhered to local institutional guidelines. Every effort was expended to ensure humane care of the animals in all animal studies.

Cell Isolation and Labeling

Cell isolation, labeling, labeling efficiency, cell viability, and fixation studies were conducted in accordance to standard procedures. Methodological details are listed as Supplementary Materials.

In Vitro and in Vivo Imaging

Label Tracking - Confocal microscopy

Temporal Labeling Kinetics: Fluorescent NPs and/or nuclear green fluorescent protein (GFP) stained cells were imaged [excitation wavelengths: λ_{green}=488 nm, λ_{red}=633 nm, emission ranges: 500–550 nm (green) and 650–700 nm (red)] using a Leica TCS SP8 confocal microscope (Leica-

Microsystems, Mainhem, UK) with HyD detectors (objective NA=1.4, 63X) at different times post-seeding (1–6 h), and at two FuGENE concentrations (25, 100 µl in 2 ml IMDM). Image post-processing was conducted using the Imaris software (Bitplane, Zurich, Switzerland) that allowed generation of three-dimensional (3D) renditions and movies showing the temporally dependent label uptake up to 6 h post-labeling.

High-content Epifluorescence Microscopy Imaging

Temporal Viability and Fluorescence: Live cells were stained with Calcein (CellTrace™ Calcein Red-Orange, Thermo Fisher Scientific, UK) for high-content imaging in 6-well plates. Independent cell cohorts (n=3, ~10–20 k cells/cohort) were maintained in culture up to 7 d (D), and a time course study (D1–D7) of live cells was conducted (at low/high proliferative rates, given initial low/high cell densities) to assess cell survival (Calcein/Hoechst), labeling efficiency (Calcein/Atto647), and fluorescence (Atto647), using a high-content imaging system (Operetta, Perkin-Elmer, Llantrisant, UK). The Operetta's Harmony software was used for image analyses.

In Vivo Cell Administration using Direct Injections

Surgical Procedure: C57BL/6 mice (adult female, 20-30 g, n=6) were anesthetized with 4% isoflurane (ISO) and placed on a heating pad, intubated, and ventilated with 100% oxygen (MiniVent, Type 845, Hugo Sachs Elektronik, Harvard Apparatus, March-Hugstetten, stroke rate of 175 strokes/min and a stroke volume of 250 µl). Analgesic was administered (80 µl, Vetergesic). A left thoracotomy was performed, and the FuGENE-labeled cells (~$1.7–2\times10^6$ CT cells in ~50 µl of IMDM media) were injected at left-ventricular (LV) myocardial sites using a

0.5 ml syringe. The chest was sutured and the intubation tubing removed to allow spontaneous breathing. Mice were monitored for 30–60 min for recovery.

MRI/MRS

All experiments were conducted on a 9.4 T Agilent scanner (Agilent Technologies, Santa Clara, CA, USA). Relevant methodological details pertaining to radiofrequency coils and in vitro studies are listed as Supplementary Materials.

In Vivo MRI

In Vivo Cardiac ^{19}F MRI and Cellular Tracking: C57BL/6 mice (n=6) were anesthetized with 4% ISO and were maintained for up to 95 min with 1.5–2.0% ISO in 100% oxygen.

All animals were placed in a specially constructed cradle and were their body temperature was maintained at ~37°C. Electrocardiographic and breathing rates were monitored using a gating system. Heart rates were maintained between 350–500 beats/min.

Six animal studies were completed in total. Three successful studies were terminal at D1, and another three were tracking studies (two mice were rescanned at D4 and D7, and one mouse at D5 and D8). Poor visualization of ^{19}F signal was evidenced in one of the tracking studies (on D7), attributed to partial mis-localization of injected cells.

Details on ^{1}H and ^{19}F image (spoiled grass) and spectroscopy (saturation recovery) acquisitions are listed as Supplementary Materials.

Image Processing

Details on image/spectral analyses are listed in the Supplementary Material section. Briefly, ^{19}F images were interpolated, colored coded, and overlaid on the anatomical ^{1}H MRI. For MRS, spectral areas were quantified.

Histology and Immunofluorescence Staining

Histology

Post-mortem histological evaluation was performed in mouse hearts on the same day following cellular implantation (terminal-D1) or at subsequent days (tracking-D7, D8) to assess the CPC injection and retention sites. The excised hearts were dehydrated and fixed (in a 4% methanol-free formaldehyde solution), processed, embedded in paraffin, and stored. Serial transverse paraffin sections of 10–17 μm were cut from base to apex, processed, and stained using the nuclear stain 4',6-diamidino-2-phenylindole (DAPI, Sigma-Aldrich, UK). Imaging and analyses were performed on a Leica bright-field optical, and on the confocal microscope, by two blinded investigators (DAPI, Atto647).

Immunofluorescence Staining

Hearts from particle-injected mice were fixed in 4% methanol-free formaldehyde solution before being transferred to 70% ethanol, followed by paraffin embedding. Hearts were sectioned (10-17 μm) and blocked for 2 h in DAKO® Protein Block (Thermo Fisher Scientific, UK). Thereafter, the sections were incubated for 2 h with goat polyclonal anti-mouse Galectin 3 antibody (RnD Systems AF1197, Oxford, UK) followed by incubation with the secondary antibody donkey anti-goat Alexa Fluor 488 (A11055, Invitrogen, Thermo Fisher Scientific, UK).

Sections were washed and mounted with Fluoromount G mounting medium (Southern Biotech 0100-01, USA) with DAPI. Images were obtained with the confocal microscope.

Statistical Analyses

All results are reported as mean ± standard deviation (SD). Two-tailed Student's t-tests (XLSTAT, Addinsoft, New York, USA), and two-way analysis of variance (ANOVA) with repeated measures (SPSS, Version 24, IBM, USA) were also used to assess mean comparisons (α=5%) (control, labeled, FuGENE-labeled, electroporated), and the effects of the labeling regime (control, labeling, FuGENE labeling), time (D1, D4, D7), and their interactions, for in vitro CDC/CT cell assays. Power calculation for the tracking studies of control, injected mice (exposure of controls p_0=0.99, relative risk of disease associated with exposure RR=0, α=5%) yielded a required minimum sample size of n=3.

3. Results

Cell Isolation and Labeling

FuGENE Optimization: Figure 1 shows sequentially gated, flow cytometric results (CT cells) (without/with FuGENE) using Atto647-fluorinated-PFCE-NPs. The labeling efficiency was > 99% (in both labeling instances) with noted increases in the total label load (D1) upon FuGENE use (>4-fold fluorescence increases with FuGENE). Successful persistence of cellular label (labeling efficiency was > 99%) was confirmed with independent FuGENE-labeled CT cell cohorts post-labeling (D8) using flow cytometry (results not shown). For the FuGENE optimization studies, the overall cell viability was >88%.

In Vitro and in Vivo Imaging

Labeling Efficiency: There is an innate heterogeneity of labeling in the studied CPCs, confounded by the label methodology (endocytosis-based internalization), cellular uptake mechanism, and the heterogeneous content of isolated cells (containing cardiac progenitors mixed with endothelial cells, fibroblasts, and others). Correspondingly, given the sensitivity disparities for flow (single cells, nm to tens of μm), epifluorescence imaging (multiple thousands of cells, tens to hundreds of μm), and MRI (cell pellets containing > 10k cells per voxel, hundreds of μm), there are expected disparities in the detection of labeled cells.

High-content Imaging

Temporal Viability and Fluorescence: Figure 2 shows quantified results for the temporally dependent proliferation and fluorescence using optical imaging of (a) FuGENE-labeled CDC and (b) CT cells at days 1 (D1), D4, and D7, at high seeding densities in vitro. The increased density of the initially seeded cells promoted enhanced proliferative activity at D4–D7 and label dilution, as reflected by the decreased levels of fluorescent intensity at D4/D7 compared to D1.

Histograms of the temporally varying cell proliferation, and mean fluorescence signal/cell, are also shown for both types of studied cells (Figure 2). The mean labeling efficiency increased to ~30–80% upon FuGENE use vs. ~5–10% following labeling (no FuGENE) ($p<0.003/p<0.0042$; CDC/CT) at day 1 (D1). However, the mean fluorescence signal decayed in labeled cells (CDC/CT) (without/with FuGENE) by D2/D4 owing to the possible cleavage of the fluorophore and cytosolic destruction of NPs (D1–D3) [Supplementary Figure S2] and cell proliferation (D4-D7) ($p<0.007/p<0.001$ for labeled, and $p<0.0002/p<0.0001$ FuGENE-labeled cases). Indicated is also the improved performance of CDCs (labeled/FuGENE-labeled) that elicit increased

fluorescent signals vs. CTs at D1 ($p<0.04/p<0.006$ CDC/CT). Two-way ANOVA with repeated measures yielded significant variability effects in viability with respect to time (CDC cells, $p=8.8\times10^{-7}$), and time ($p=1\times10^{-7}$), labeling scheme ($p=0.01$), and their interactions ($p=0.002$) (CT cells). Correspondingly, significant variability effects in fluorescence were noted for both cell types (CDC/CT) in terms of time ($p=0.002/1.8\times10^{-5}$), labeling scheme ($p=1.4\times10^{-7}/4.4\times10^{-11}$), and their interactions ($p=5.6\times10^{-6}/5.2\times10^{-10}$).

Electroporation: Similar viability/fluorescence trends to those in Figure 2 were observed for FuGENE-labeled compared to electroporated cells seeded at low densities [Figure 3 (A, B)]. By D7, viability was higher for electroporated cells vs. FuGENE-labeled cells ($p<0.04$), but the initial fluorescence response was better for FuGENE-labeled cells ($p<0.002$, D1). However, the mean fluorescence signal decayed significantly in both cell types (electroporated and with FuGENE) by D4 as cells proliferated ($p<0.025$, D1 vs. D4 for electroporated, and $p<0.002$, D1 vs. D4 FuGENE-labeled cases).

Label Tracking - Confocal microscopy

Temporal Labeling Kinetics: Figure 4(A-F) shows phase contrast confocal microscopy images of GFP positive CPCs, and (B, C) enlarged views of CPCs post-FUGENE labeling with low (25 μl), and high doses (100 μl) (red color). Figure 4(D–F) depicts 3D renditions of cells, (D) label localization (no FuGENE), and (E, F) labeled cells with 25 and 100 μl of FuGENE. As indicated, cluster formation prohibits label uptake at high FuGENE doses [Figure 4(C, F)]. This problem is ameliorated at lower/optimal dose levels (Figure 4(B, E)). Supplementary Figure S2 contains three movies that confirm the temporal labeling kinetics using confocal live cell imaging (Movie

1: cellular labeling at 1.2 h post-label administration, Movie 2: cellular label with FuGENE with 25 µl per million cells at 5.7 h, and Movie 3: high FuGENE dose with 100 µl per million cells at 4.15 h). Significant label uptake was confirmed within 2–3 h post-label administration in all cases.

MRI/MRS

^{19}F-MRI/MRS: Figure 4 shows unlocalized ^{19}F MRS of TFA and labeled cells without/with FuGENE indicating signal increases from NPs (G–I), label localization at low doses (H), and an increased signal when the label is predominantly extracellular (I). Figure 4(J, K) shows axial ^{19}F MRI from labeled CPCs in pellet suspensions at low/high FuGENE doses (butterfly coil). The results from MRS/MRI (Figure 4(G–K)) confirm confocal findings. Specifically, low label uptake is manifested by simple labeling (Figure 4(G)) that significantly enhances upon FuGENE dose increases (Figure 4(H, I)). The localization of FuGENE-encapsulated NPs in the extracellular space at nonoptimal FuGENE doses justifies the increased signal.

Confirmation of the label uptake mechanism and label localization attributed to FuGENE is provided by separate control experiments (Supplementary Figure S3(A–D)). In this figure, ^{19}F MRS control phantom tests are summarized, confirming the source of the fluorine signal increase due to FuGENE. Independent in vitro labeling/FuGENE experiments were conducted (solenoid coil with a homogeneous B_1 response) for the quantification of ^{19}F concentrations with respect to the concentration of a TFA standard (50 mM). Table 1 summarizes the SNR, cell seeding density, labeling efficiency, and ^{19}F concentrations. As shown, indicative 4-8-fold concentration improvements (0.3 vs. 1.4–2.5 mM) are achieved with FuGENE, yielding corresponding labeling efficiency increases (10 vs. 44–75%).

Furthermore, comparison of the unlocalized, in vitro ^{19}F spectra from electroporated and FuGENE-labeled CT cells (butterfly coil) indicates a 125-fold signal (D1) increase with FuGENE labeling compared to electroporation (Supplementary Figure S4 (A, B)). FuGENE-labeled cells following electroporation yielded 10% higher signal compared to FuGENE-labeled cells (Supplementary Figure S4 (C, D)).

In Vivo Cardiac ^{19}F MRI, Tracking, and Quantification: Figure 5 shows overlaid ^{1}H MRI with ^{19}F for terminal studies and bright field histology, confirming the injection locations. High-resolution, gated ^{1}H MRI are shown in Figure 6(A–F), and a sequence of overlaid $^{1}H/^{19}F$ MRI of ~1.7–2 million FuGENE-labeled cells injected in the antero-lateral ventricular myocardium (D1, D4, and D8). Localization of the enhanced ^{19}F signal regions was confirmed with histological staining, as described below.

Quantification: Temporal ^{19}F voxel signal decreases were noted in vivo at increasing time intervals post-CPC administration, whereby the evoked ^{19}F signal progressively diminished to ~31% of its value after injections, over a period of 7-8 days (Figures 6–7).

Histology: Typical bright field, and confocal microscopy imaging (nuclear [DAPI], label [Atto648], macrophages [Gal3]) are shown for a terminal (D1), and tracking studies (D7 or D8) confirming retention/localization of injected cells (D1), and infiltration of macrophages (Gal3) in fixed hearts at D7/D8 (Figure 8).

4. Discussion

Hitherto direct labeling methods led to an overall low and heterogeneous label uptake that prohibited cost-efficient, fast, and practical ^{19}F MRI visualization and tracking of labeled SCs in cardiac applications.

Our choice of FuGENE versus protamine-sulphate, electroporation, or other transfection agents (e.g., lipofectamine) was based on the increased CPC viability and label uptake compared to those observed in preliminary experimental protamine-sulphate and lipofectamine studies (data not shown). Labeling was measured by flow cytometry (indicating label persistence at D8) and optical microscopy.

The observed discrepancy of the labeling efficiency of flow cytometry and epifluorescence imaging is attributed to the detection sensitivity differences of the two modalities. Flow represents a highly sensitive, single-cell-based optical method, while epifluorescence microscopy relies on volume-averaged optical signal responses from hundreds of cells. Epifluorescence imaging and MRI exhibited higher cellular sensitivity detection thresholds than flow cytometry, as reported below. This suggests that the level of labeling in many of the cells detected by flow cytometry would be too low to be detected using MRI.

Temporal kinetic studies in single cells indicate that NPs localize within FuGENE vesicles within the first 3-4 h, however, high doses lead to aggregate formations in the extracellular space, resulting in a low-label uptake, whereas the low-label dose achieved increased intracellular uptake, as confirmed by confocal microscopy. Based on recent MRI work [29], the in vitro load detection threshold for ^{19}F PFCE labels (using cells and TFA) was 0.5 mM (butterfly). Additionally, the efficiency of labeling with FuGENE increased by 4.4–7.5 times vs. simple labeling yielding corresponding ^{19}F concentration improvements in the order of 1.4–2.5 mM. Correspondingly, SNR increases in the order of 4.4–14 times were noted in ^{19}F MR images

in vitro compared to the simple labeling case. Imaging can thus be executed within a few min using conventional gradient echo pulse sequences [29]. Signal enhancements may be highly beneficial in minimizing cell label load and potential toxicity in applications of cardiac pathology in vivo.

The fluorescent intensity decreased within 2-4 days in cultures in vitro primarily as a result of fluorophore cleavage, secondary to subsequent proliferation and label dilution (following day 3). Despite the slightly reduced viability rate following labeling with FuGENE (compared to labeling without it, or electroporation), the proliferative capacity of cells recovered. Notably, the persistence of in vivo MRI signal relies on the long-term fates of the NPs. The migratory paths of endosome-packaged NPs within cells involved lysosomal destruction and exocytosis, the temporal evolution of this process was faster than the timescale of cell division.

Several primary mechanisms may cause changes to cellular status (and possibly to the evoked signal) with time including possible: a) cellular migration/dispersion and clearance through the microcirculation, b) cell death, c) macrophage infiltration and label/cellular debris scavenging, and e) hypoxic-induced proliferation (no signal change). Ultimately, physiologically/pathologically relevant mechanisms supersede. For example, during cultures in vitro, cells proliferate and dilute label (as indicated herein). Under ischemic conditions, cells may undergo an initial, hypoxia-induced proliferation, causing label dilution but minimal overall ^{19}F signal changes. Alternatively, cells may disperse and migrate from the injection site, ultimately entering the microcirculation, or lyse, and release the label into the extracellular space, thereby causing fluorescence, or possible ^{19}F MRI signal decreases. The infiltration of macrophages at later times post-injection will also initiate cellular and label scavenging. While the end-effect is a

complex interplay of the proposed mechanisms, in almost all cases, temporally dependent, voxel-induced signal decreases are expected, justified by in vivo findings.

In terms of quantification, the evoked signal on days subsequent to the day of injection may arise from both viable cells, macrophage-endocytosed NPs that remain at the injection site, and extracellularly released NPs from lysed CPCs. While noninvasive, single voxel ^{31}P metabolic MRS may be able to assess the viability of injected cells [30], its potential applicability is limited by spatial resolution since CPCs will likely disperse, migrate, or lyse, post-injection. Combination of bioluminence techniques with MRI may address such issues, however, preclinical acquisition protocols become complex.

While the consistency of localization/detection of injected cells in the myocardium using ^{19}F MRI has been confirmed with histology at the end of D1 post-CPC injection, the major limitations of this work include the limited animal sample size in tracking studies, and the lack of additional immunohistochemical analyses required for the detailed investigation of the spatio-temporal evolution of signal changes, including the confirmation of label localization within the interstitial space, within recruited macrophages, and/or the microvasculature.

Despite these shortcomings, we have demonstrated fast, in vivo cardiac ^{19}F MRI post-SC injections in the in vivo mouse. More importantly, the protocol for cell preparation and injection has potential to be directly translatable to the clinic. The cell types employed herein have been used before with success in animal/human studies of cardiac pathology [26, 27]. However, additional issues ought to be resolved first (cell density, administration route, optimization of cell preparation methodologies for large-scale use) drawing on knowledge from successful strides based on localized injections of dendritic cells in humans [31, 32]. No potential problems are envisaged in terms of ^{19}F label release and the safety profile of NPs, since the doses are small

and since all of these components have been previously used in humans with no reported adverse toxic effects [32]. PFCEs are inert, they are not metabolized in vivo, and will be excreted through exhalation in the lungs, and through the liver, spleen, kidneys, and blood, as has been previously been reported [33, 31]. It is understood that a long-clearance time is unacceptable in clinical studies, as has been observed in prior murine studies using high-dose PFCE emulsions [34]. Nevertheless, additional work needs to be expended to address clearance times for the trace amounts of PFCEs used herein in labeled cells, as it is unrealistic to extrapolate prior inferences based on prior dendritic cell studies.

The methodology may be further developed clinically as a noninvasive tool for determining the successful CPC administration type and route [35] and the temporally dependent retention in the acute phases of myocardial infarction.

Acknowledgements

We are thankful to Dr. J. Brown, Dr. A. Worth, and Dr. M. Benson, for their support and guidance with the cell cultures, flow cytometry studies, and FuGENE control studies. Particular thanks are attributed to Dr. A. Rai at U. Coimbra, Portugal, for useful discussions on the electroporation protocol.

We also thank Mrs. H. Gray, Dr. M. Maguire, Mrs. L. Stork, and Ms. A. Vernet, for their help with the in vivo studies, and for useful discussions on the control FuGENE MRS, use of the solenoid coil, and IDL processing (Dr. M. Maguire).

Dr. Petros Patsali at the Cyprus Institute of Neurology and Genetics, Nicosia, Cyprus, is thanked for his assistance with optical/fluorescence imaging.

Author contributions

Guarantors of integrity of entire study: CC, MS, EMcN, CAC, JP, RSU, RC, AA, SPP, KK

Study concepts/study design: CC, MS, EMcN, CAC, SPP, JP, RSU

Data acquisition: CC, EMcN, AA, AS, RSU

Data analysis/interpretation: CC, EMcN, RSU, SPP, CAC, MS, RC, AA, AS, JP, KK, AH, LP, RA

Manuscript drafting: CC

Manuscript revision for important intellectual content: CC, CAC, MS, EMcN, RC, RSU, AS, JP, RSU, SPP, AA, KK, AH, LP, RA

Approval of final version of submitted manuscript: all authors

Agrees to ensure any questions related to the work are appropriately resolved: CC

Literature research: CC

Experimental studies: CC, AA, RSU, EMcN, AS, JP, ES

Statistical analysis: CC

Manuscript editing: CC, CAC, EMcN, MS, RSU

Role of the Funding Source

The funding sources had no role in the study design, collect, analysis, and interpretation of the data, the writing of the report, and in the decision to submit the article for publication.

Disclosures

There are no disclosures.

Competing Financial Interests

None.

References

1. Taylor DA, Chandler AM, Gobin AS, Sampaio LC. Maximizing cardiac repair should we focus on the cells or on the matrix? Circulation Research 2017; **120**:30–32.

2. Feyen DA, Gaetani R, Doevendans PA, Sluijter JP. Stem cell-based therapy: Improving myocardial cell delivery. Advanced Drug Delivery Reviews 2016; **106(PtA)**:104–115. doi: 10.1016/j.addr.2016.04.023.

3. Mitragotri S, Anderson DG, Chen X, Chow EK, Ho D, Kabanov AV, et al. Accelerating the Translation of Nanomaterials in Biomedicine. ACS Nano 2015; **9(7)**:6644–54. doi: 10.1021/acsnano.5b03569.

4. Lewin M, Carlesso N, Tung CH, Tang XW, Cory D, Scadden DT, et al. Tat peptide-derivatized magnetic nanoparticles allow in vivo tracking and recovery of progenitor cells. Nature Biotechnology 2000; **18**:410–414.

5. Hoehn M, Kustermann E, Blunk H, Wiedermannm D, Trapp T, Wecker S, et al. Monitoring of implanted stem cell migration in vivo: a highly resolved in vivo magnetic resonance imaging investigation of experimental stroke in rat. Proceedings of the National Academy of Sciences 2002; **99(25)**:16267–16272.

6. Ahrens ET, Flores R, Xu H, Morel PA. In vivo imaging platform for tracking immunotherapeutic cells. Nature Biotechnology 2005; **23(8)**:983–987.

7. Srinivas M, Morel PA, Ernst LA, Laidlaw DH, Ahrens ET. Fluorine-19 MRI for visualization and quantification of cell migration in a diabetes model. Magnetic Resonance in Medicine 2007; **58**:725–734.

8. Shin SH, Kadayakkara DK, Bulte JW. In Vivo ^{19}F MR imaging cell tracking of inflammatory macrophages and site-specific development of colitis-associated dysplasia. Radiology 2017; **282(1)**:194–201.

9. Bertorelle F, Wilhelm C, Roger J, Gazeau F, Menager C, Cabuil V. Fluorescence-modified superparamagnetic nanoparticles: intracellular uptake and use in cellular imaging. Langmuir 2006; **22(12)**:5385–91.

10. Arbab AS, Bashaw LA, Miller BR, Jordan EK, Lewis BK, Kalish H, et al. Characterization of biophysical and metabolic properties of cells labeled with superparamagnetic iron oxide nanoparticles and transfection agent for cellular MR imaging. Radiology 2003; **229**:838–846.

11. Arbab AS, Yocum GT, Lakish H, Jordan EK, Anderson SA, Khakoo AY, et al. Efficient magnetic cell labeling with protamine sulfate complexed to ferumoxides for cellular MRI. Blood 2004; **104(4)**:1217–1223.

12. Arbab AS, Yocum GT, Rad AM, Khakoo AY, Fellowes V, Read EJ, et al. Labeling of cells with ferumoxides-protamine sulfate complexes does not inhibit function or differentiation capacity of hematopoietic or mesenchymal stem cells. NMR in Biomedicine 2005;**18**:553–559.

13. Frank JA, Miller BR, Arbab AS, Zywicke HA, Jordan EK, Lewis BK, et al. Clinically applicable labeling of mammalian and stem cells by combining superparamagnetic iron oxides and transfection agents. Radiology 2003; **228(2)**:480–7.

14. Thu MS, Bryant HL, Coppola T, Jordan EK, Budde MD, Lewis BK, et al. Self-assembling nanocomplexes by combining ferumoxytol, heparin and protamine for cell tracking by magnetic resonance imaging. Nature Medicine 2012; **28(3)**:463–468.

15. Srinivas M, Cruz LJ, Boneto F, Heerschap A, Figdor CG, de Vries IJM. Customizable, multi-functional fluoricarbon nanoparticles for quantitative in vivo imaging using ^{19}F MRI and optical imaging. Biomaterials 2010; **31**:7070–7077.

16. Jing Y, Mal N, Williams PS, Mayorga M, Penn MS, Chalmers JJ, et al. Quantitative intracellular magnetic nanoparticle uptake measured by live cell magnetophoresis. FASEB Journal 2008; **22**:4239–4247.

17. Barnett BP, Ruiz-Cabello J, Hota P, Liddell R, Walczak P, Howland V, et al. Fluorocapsules for improved function, immunoprotection, and visualization of cellular therapeutics with MR, US, and CT imaging. Radiology 2011; **258(1)**:182–191.

18. Han NR, Lee H, Baek S, Yun JI, Park KH, Lee ST. Delivery of episomal vectors into primary cells by means of commercial transfection reagents. Biochemical and Biophysical Research Communications 2015; **461**:348–353.

19. Ferreira L, Karp JM, Nobre L, Langer R. New opportunities: the use of nanotechnologies to manipulate and track stem cells. Cell Stem Cell 2009; **3**:136–146.

20. Aday S, Paiva J, Sousa S, Gomes RSM, Pedreiro S, So PW, et al. Inflammatory modulation of stem cells by Magnetic Resonance Imaging (MRI)-detectable nanoparticles. RSC Advances 2014; **4**:31706–31709.

21. Luo D, Saltzman WM. Synthetic DNA delivery systems. Nature Biotechnology 2000; **18**:33–37.

22. Gomes RSM, das Neves RP, Cochlin L, Lima A, Carvalho R, Korpisalo P, et al. Efficient pro-survival/angiogenic miRNA delivery by an MRI-detectable nanomaterial. ACS Nano 2013; **7(4)**:3362–3372.

23. Carr CA, Stuckey DJ, Tan J, Tan SC, Gomes RSM, Camelliti P, et al. Cardiosphere-derived cells improve function in the infarcted rat heart for at least 16 weeks – an MRI study. PLoS ONE 2011; **6(10)**:e25669.

24. Constantinides C, McNeill E, Benson M, Urruela RS, Padilla S, Malandraki-Miller S, et al. Improvements in the cellular uptake of perfluorocarbon nanoparticles and ^{19}F MRS/MRI detectability using the transfection agent FuGENE. ISMRM Workshop on Molecular and Cellular MRI: Focus on Integration: Amsterdam, Netherlands, June 2016.

25. Constantinides C, Maguire M, Stork L, Swider E, Srinivas M, Carr AC, et al. Temporal accumulation and localization of isoflurane in the C57BL/6 mouse and assessment of its potential contamination in ^{19}F MRI with perfluoro-crown ether-labeled cardiac progenitor cells at 9.4 T. JMRI December 2016. DOI: 10.1002/jmri.25564.

26. Makkar R, Smith RR, Cheng K, Malliaras K, Thomson L, Berman D, et al. Intracoronary cardiosphere-derived cells for heart regeneration after myocardial infarction (CADUCEUS): a prospective, randomised phase 1 trial. Lancet 2012; **379(9819):**895–904. http://www.thelancet.com/journals/lancet/article/PIIS0140-6736(12)60195-0/fulltext.

27. Perbellini F, Gomes RS, Vieira S, Buchanan D, Malandraki-Miller S, Bruyneel AA, et al. Chronic high-fat feeding affects the mesenchymal cell population expanded from adipose tissue but not cardiac atria. Stem Cells Transl Med. 2015; **4(12)**:1403–14. DOI: 10.5966/sctm.2015-0024.

28. S. Malandraki-Miller, R. Tyser, P. Riley P, C.A. Carr. Comparative characterization of cardiac atrial progenitor cell populations for use in cell therapy, Heart **100** (2014) A14.

29. Constantinides C, Maguire ML, McNeill E, Carnicer R, Swider E, Srinivas M, et al. Fast, Quantitative ^{19}F MRI/MRS of PFCE-labeled progenitor stem cells and macrophages at 9.4T. PLOS One 2018; **13(1)**: e0190558.

30. Manganas LN, Zhang X, Li Y, Hazel RD, Smith SD, Wagshul ME, et al. Magnetic resonance spectroscopy identifies neural progenitor cells in the live human brain. Science 2007; **318(5852)**: 980–5.

31. Srinivas M, Heerschap A, Ahrens ET, Figdor CG, de Vries IJ. ^{19}F MRI for quantitative in vivo cell tracking. Trends Biotechnology 2010; **28(7)**:363–70. doi: 10.1016/j.tibtech.2010.04.002. Epub 2010 Apr 26.

32. Srinivas M, Cruz LJ, Bonetto F, Heerschap A, Figdor CG, de Vries IJ. Customizable, multi-functional fluorocarbon nanoparticles for quantitative in vivo imaging using ^{19}F MRI and optical imaging. Biomaterials 2010; **27**:7070–7. doi: 10.1016/j.biomaterials.2010.05.069.

33. Amiri H, Srinivas M, Veltien A, van Uden MJ, de Vries IJ, Heerschap A. Cell tracking using ^{19}F magnetic resonance imaging: technical aspects and challenges towards clinical applications. European Radiology 2015; **25(3)**:726–35. doi: 10.1007/s00330–014–3474–5.

34. Srinivas M, Boehm-Sturm P, Figdor CG, de Vries IJ, Hoehn M. Labeling cells for in vivo tracking using ^{19}F MRI. Biomaterials. 2012; **33(34)**:8830–40. doi: 10.1016/j.biomaterials.2012.08.048.

35. Ye Y, Wang C, Zhang X, Hu Q, Zhang Y, Liu Q, Wen D, Milligan J, Bellotti A, Huang L, Dotti G, Gu Z. A melanin-mediated cancer immunotherapy patch. Sci Immunology 2017; **2(17)**: pii: eaan5692. doi: 10.1126/sciimmunol.aan5692.

Tables

Table 1: SNR of ^{19}F MRI from labeled and transfected CT cells (at an optimal FuGENE dose), and mean fluorine concentration per cell (based on MRS) using the solenoid coil. Concentrations of labeled samples were estimated using an external reference TFA solution (50 mM), and ranged between 0.3–2.5 mM, respectively.

Biomarker / **Sample**	**Relaxation Times (T_1/T_2) (ms)**	**^{19}F MRI Signal-to-noise-ratio (SNR)**	**Cell Seeding Density**	**Labeling Efficiency (%)**	**^{19}F Concentration (mM)**
TFA (50 mM)	2728/2365[¥]	—	—	—	50
NP (solution)[*]	773/360	—	—	—	3.3
Labeled CT	1324/NA	27	$\sim 10^6$	10	0.3
FuGENE-labeled CT[†]	1360/533	103–373	$\sim 10^6$	44–75	1.4–2.5

[*]Results denote an average of two independent measurements

[†]Improvements in SNR in the order of 4–14 times are achieved using FuGENE-labeling compared to simple labeling

[¥]Results reproduced from Constantinides et al. [29]

Figure Captions

Figure 1: **Flow cytometric results of CDCs**. Side scatter (SSC) vs. forward side scatter (FSC) (CT cells) and side scatter vs. side scatter plots (singlets vs. doublets) in justification of the successful implementation of the labeling protocol without and with FuGENE (on day 1 [D1] post-labeling). The cells were labeled with PFCE-NPs containing Atto647. Successful persistence of cellular label was confirmed with independent CT cell cohorts on D8 post-labeling using flow cytometry (results not shown).

Figure 2: **Temporal quantification of control, labeled and FUGENE-labeled CDCs.** Temporally dependent proliferation, and fluorescence response (Calcein, Atto647) using optical-epifluorescence imaging of FuGENE-labeled cells at days 1 (D1), D4, and D7, at a high seeding density. Increased cell density promotes proliferative activity at D4–D7 and label dilution, as reflected by the decreased levels of fluorescent intensity. Histograms of temporally dependent proliferation, and mean fluorescence intensity for (A, B) CDC (n=3), and (C, D) CT cells (D1–D7) (n=3). Epifluorescence studies of unlabeled control cells conducted in (B, D) did not elicit fluorescent signals (detected signal values were only attributed to autofluorescence and noise – not shown). Mean control fluorescence signals (unlabeled cells) matched the elicited mean fluorescence signals from labeled cells at D4–D7.

Figure 3: **Quantification of FUGENE-labeled and electroporated CDCs.** (A, B) Histograms of temporally dependent proliferation and mean fluorescence intensity

(Calcein, Hoechst, Atto647) for FuGENE-labeled and electroporated-labeled CT cells (D1-D7) plated at low-seed densities in correlation to epifluorescence imaging (n=3). Increased proliferative activity promoted label dilution at D4-D7, as reflected by the decreased levels of fluorescent intensity. Mean control fluorescence signals (unlabeled cells) matched elicited mean fluorescence signals from labeled (FuGENE, electroporated) cells at D4-D7.

Figure 4: **Validation of label localization in CDCs using confocal microscopy and ^{19}F MRS/MRI.** (A) Phase contrast (PC) confocal microscopy of cardiac progenitor cells (CPCs), (B, C) CPCs post-labeling with 25 (intracellular - white arrows) and 100 μl (extracellular - grey arrows) of FuGENE, (D-F) corresponding label localization in (D) labeled cells, (E, F) and labeled cells with 25 and 100 μl of FuGENE. Green and red colors respectively indicate nuclear GFP and perfluoro-crown (PFCE) NP label fluorescence. (G-I) Unlocalized ^{19}F magnetic resonance spectroscopy (MRS) of trifluoro-acetic acid (TFA) and labeled cells with and without and with transfection FuGENE indicating signal increases from NPs post-transfection (H, I) label localization at low doses (H), and a spectral shift when the label is predominantly extracellular (I); (J, K) Corresponding axial ^{19}F MRI from labeled CPCs in pellet suspensions at low/high transfection FuGENE doses (butterfly coil).

Figure 5: **In vivo cardiac ^{19}F MRI of intramyocardially injected FUGENE-labeled CDCs and bright field histological validation.** (A-F) Representative, ungated ^{19}F views superimposed on ungated anatomic ^{1}H for two terminal studies. (G, H) Shown also are bright-field histological images identifying the location of the

injection sites (window/level settings for ^{19}F images are different for different views).

Figure 6: **In vivo cardiac ^{19}F MRI tracking and temporal signal quantification.** (A, F) In vivo, gated ^{1}H and ungated oblique $^{1}H/^{19}F$ MRI of the heart following a surgical procedure of cell injection (butterfly coil). The sequence of cardiac ^{19}F MRI depicts views with narrow receiver bandwidth (1–3 kHz) acquisitions identifying the prolonged and contributory effects of ISO anesthesia, as reported earlier by Constantinides et al. [25] (window and level settings for ^{19}F are different for different views). (G, H) Normalized histograms of the spectral areas of ISO and labeled cells (gated/ungated) at D1 (n=3, 4–6 h post-surgery), D4–D5 (n=3), and D7–D8 (n=2), and (I) corresponding normalized histogram of ^{19}F signal from the entire volume of the detected, hyperenhanced regions at the injection sites with respect to the total fluorine signal on D1 [Note that three mice were imaged in the D7–D8 group but signal was only detected in two].

Figure 7: **Proposed models of temporally dependent ^{19}F decreases in tracking studies.** Schematics represent typical image voxels containing injected, labeled CPCs, apoptotic CPCs, macrophages, and PFCE-NPs, and the prominent mechanisms that may affect voxel-volume averaged signal intensity, as these modulate intracellular/extracellular volume and fluorine content. Possible relaxation changes (T_1, T_2) are ignored. Symbols S_{ave} denote average signal intensities, V volumes (intracellular, vesicular, macrophage), and [^{19}F] fluorine concentrations. Indices k, l, m, and n, denote symbols for real numbers that quantify intracellular volume or fluorine changes within the voxel.

Figure 8: **Nuclear, bright field histological and immunostaining imaging.** (A–E) Histological unstained and stained sections of murine hearts in justification of the retention of injected labeled cells, based on nuclear (DAPI), and surface marker (Atto647) staining (bright spots) using confocal imaging. (C) Histological/stained short-axis, mid-apical views of three murine hearts ([A–D] terminal experiments in two mice at (A, B) 4 and (C, D) 6 h post-cell injection on day 1 (D1), and [E–H] on D7/D8) indicating the sites of injected CPCs using bright field (C, D, E, H), nuclear (A), surface (B, E, Atto647), and immunostaining (F-G, Galectin3 (Gal3)), using confocal imaging.

Figures

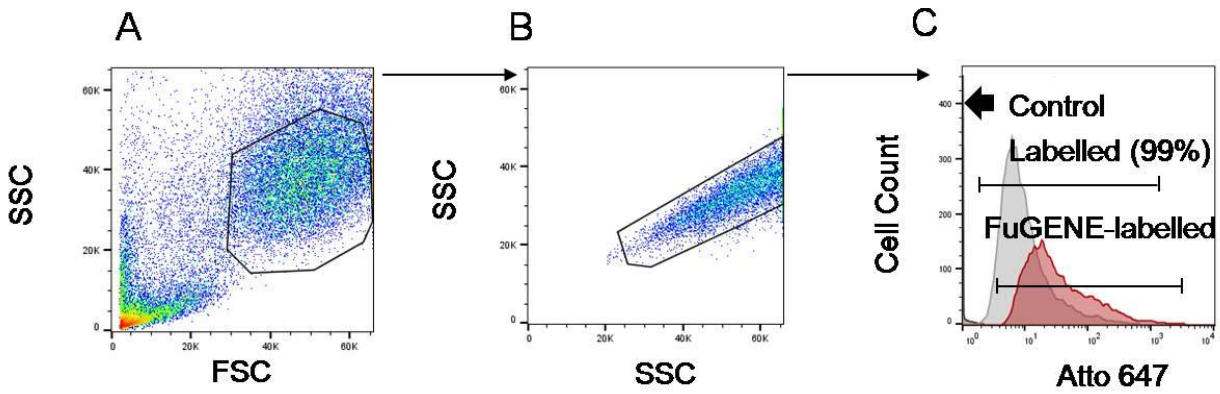

Figure 1: Flow cytometric results of CDCs. Side scatter (SSC) vs. forward side scatter (FSC) (CT cells) and side scatter vs. side scatter plots (singlets vs. doublets) in justification of the successful implementation of the labeling protocol without and with FuGENE (on day 1 [D1] post-labeling). The cells were labeled with PFCE-NPs containing Atto647. Successful persistence of cellular label was confirmed with independent CT cell cohorts on D8 post-labeling using flow cytometry (results not shown).

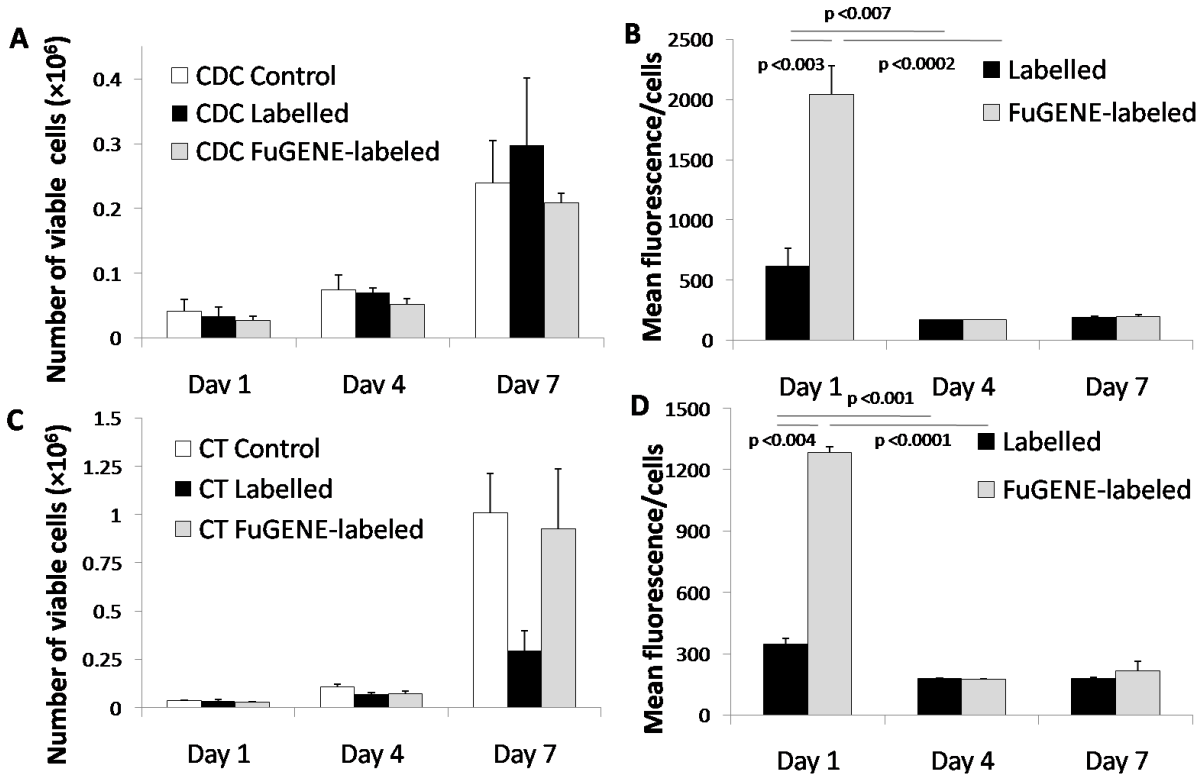

Figure 2: Temporal quantification of control, labeled and FUGENE-labeled CDCs. Temporally dependent proliferation, and fluorescence response (Calcein, Atto647) using optical-epifluorescence imaging of FuGENE-labeled cells at days 1 (D1), D4, and D7, at a high seeding density. Increased cell density promotes proliferative activity at D4–D7 and label dilution, as reflected by the decreased levels of fluorescent intensity. Histograms of temporally dependent proliferation, and mean fluorescence intensity for (A, B)

CDC (n=3), and (C, D) CT cells (D1–D7) (n=3). Epifluorescence studies of unlabeled control cells conducted in (B, D) did not elicit fluorescent signals (detected signal values were only attributed to autofluorescence and noise – not shown). Mean control fluorescence signals (unlabeled cells) matched the elicited mean fluorescence signals from labeled cells at D4–D7. Statistical significance bars are not shown in A and C (CDC: Control-D1 vs. D7, $p<0.007$, D4 vs. D7, $p<0.014$; Labelled-D1 vs. D4, $p<0.021$, D4 vs. D7, $p<0.019$, D1 vs. D7, $p<0.012$; FuGENE-labeled: D1 vs. D7, $p<0.001$, D4 vs. D7, $p<0.006$; and CT: Control-D1 vs. D4, $p<0.002$, D4 vs. D7, $p<0.002$, D1 vs. D7, $p<0.001$; Labeled-D1 vs. D4, $p<0.009$, D4 vs. D7, $p<0.019$, D1 vs. D7, $p<0.012$; FuGENE-labeled: D1 vs. D7, $p<0.008$, D4 vs. D7, $p<0.009$; Controlled vs. labeled (D4), $p<0.022$, (D7), $p<0.06$; Controlled vs. FuGENE-labeled (D4), $p<0.047$, (D7), $p<0.030$).

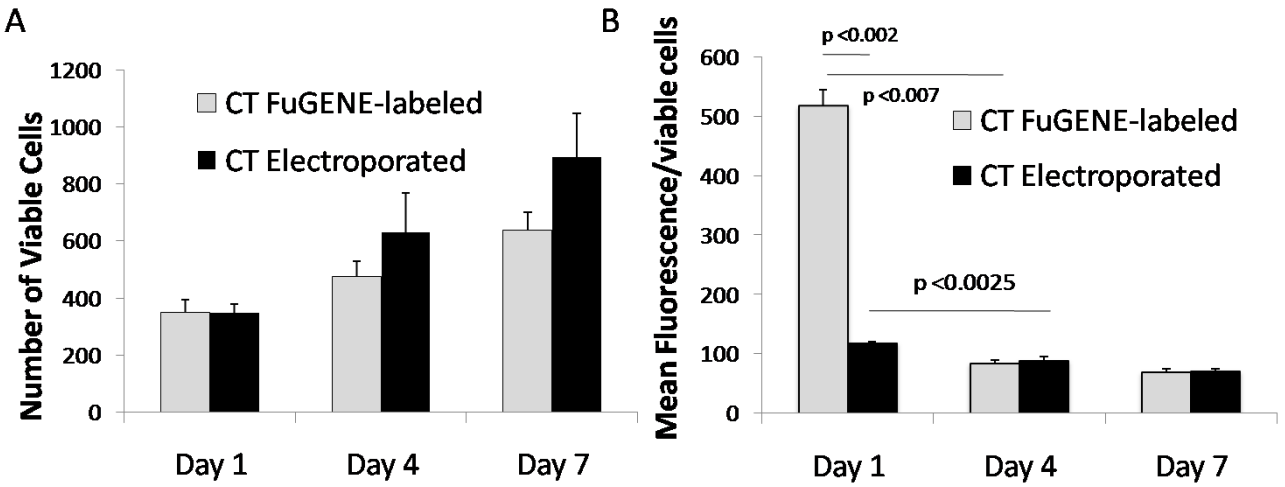

Figure 3: Quantification of FUGENE-labeled and electroporated CDCs. (A, B) Histograms of temporally dependent proliferation and mean fluorescence intensity (Calcein, Hoechst, Atto647) for FuGENE-labeled and electroporated-labeled CT cells (D1-D7) plated at low seed densities in correlation to epifluorescence imaging (n=3). Increased proliferative activity promoted label dilution at D4-D7, as reflected by the decreased levels of fluorescent intensity. Mean control fluorescence signals (unlabeled cells) matched elicited mean fluorescence signals from labeled (FuGENE, electroporated) cells at D4-D7. Statistical significance bars are not shown in A (CT-FuGENE-labeled: D1 vs. D4, $p<0.035$, D4 vs. D7, $p<0.027$, D1 vs. D7, $p<0.003$; CT Electroporated: D1 vs. D4, $p<0.025$, D1 vs. D7, $p<0.004$).

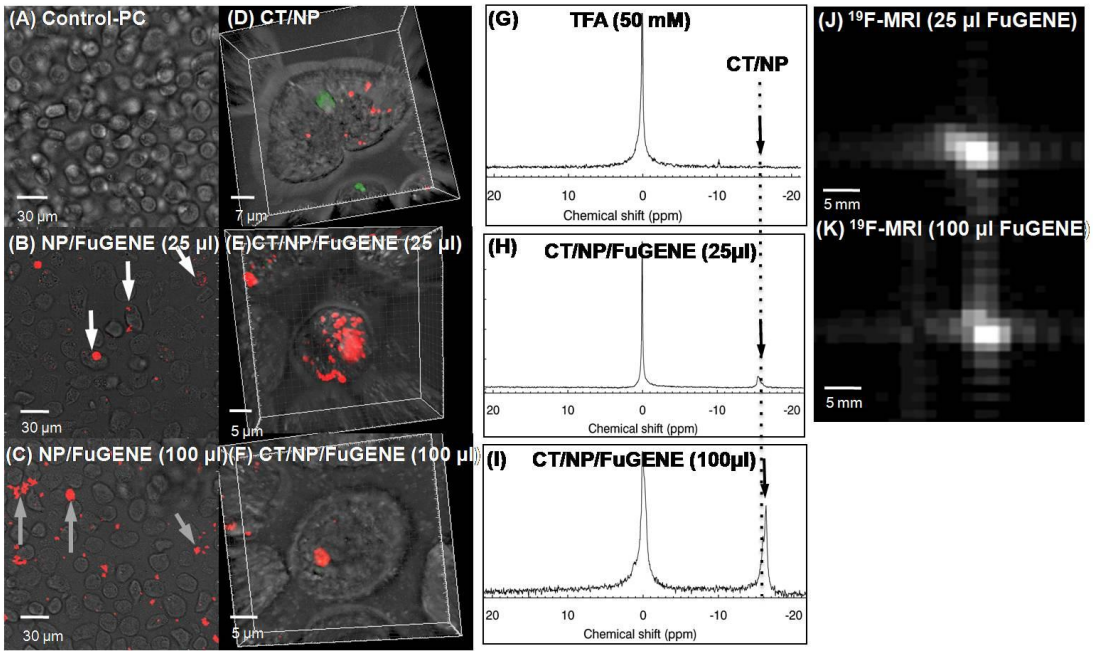

Figure 4: Validation of label localization in CDCs using confocal microscopy and ^{19}F MRS/MRI. (A) Phase contrast (PC) confocal microscopy of cardiac progenitor cells (CPCs), (B, C) CPCs post-labeling with 25 (intracellular - white arrows) and 100 µl (extracellular - grey arrows) of FuGENE, (D-F) corresponding label localization in (D) labeled cells, (E, F) and labeled cells with 25 and 100 µl of FuGENE. Green and red colors respectively indicate nuclear GFP and perfluoro-crown (PFCE) NP label fluorescence. (G-I) Unlocalized ^{19}F magnetic resonance spectroscopy (MRS) of trifluoro-acetic acid (TFA) and labeled cells with and without and with transfection FuGENE indicating signal increases from NPs post-transfection (H, I) label localization at low doses (H), and a spectral shift when the label is predominantly extracellular (I); (J, K) Corresponding axial ^{19}F MRI from labeled CPCs in pellet suspensions at low/high transfection FuGENE doses (butterfly coil).

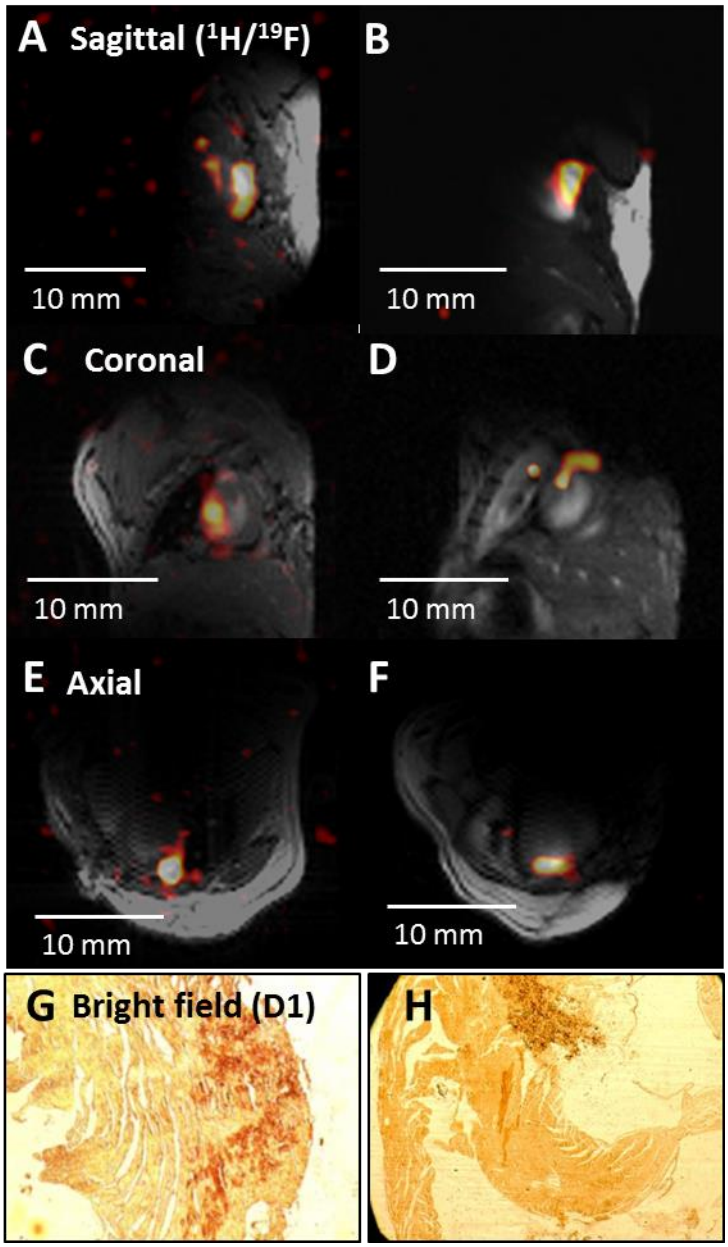

Figure 5: In vivo cardiac ^{19}F MRI of intramyocardially injected FUGENE-labeled CDCs and bright field histological validation. (A-F) Representative, ungated ^{19}F views superimposed on ungated anatomic ^{1}H for two terminal studies. (G, H) Shown also are bright-field histological images identifying the location of the injection sites (window/level settings for ^{19}F images are different for different views).

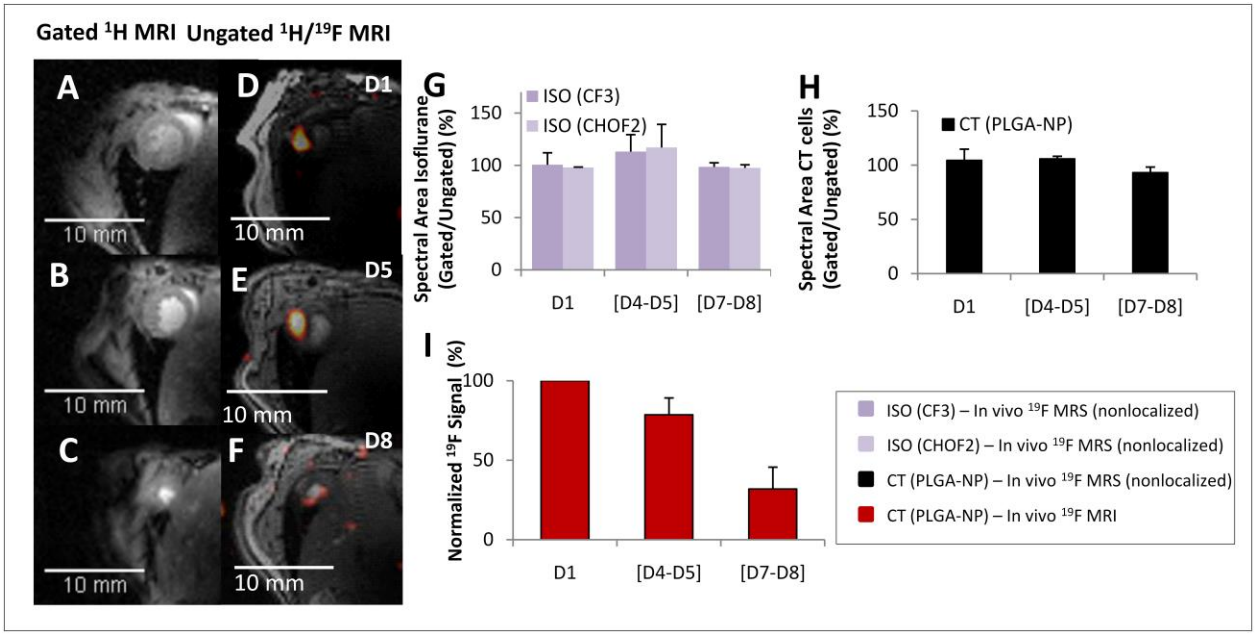

Figure 6: In vivo cardiac ^{19}F MRI tracking and temporal signal quantification. (A, F) In vivo, gated ^{1}H and ungated oblique ^{1}H/^{19}F MRI of the heart following a surgical procedure of cell injection (butterfly coil). The sequence of cardiac ^{19}F MRI depicts views with narrow receiver bandwidth (1–3 kHz) acquisitions identifying the prolonged and contributory effects of ISO anesthesia, as reported earlier by Constantinides et al. [25] (window and level settings for ^{19}F are different for different views). (G, H) Normalized histograms of the spectral areas of ISO and labeled cells (gated/ungated) at D1 (n=3, 4–6 h post-surgery), D4–D5 (n=3), and D7–D8 (n=2), and (I) corresponding normalized histogram of ^{19}F signal from the entire volume of the detected, hyperenhanced regions at the injection sites with respect to the total fluorine signal on D1 [Note that three mice were imaged in the D7–D8 group but signal was only detected in two].

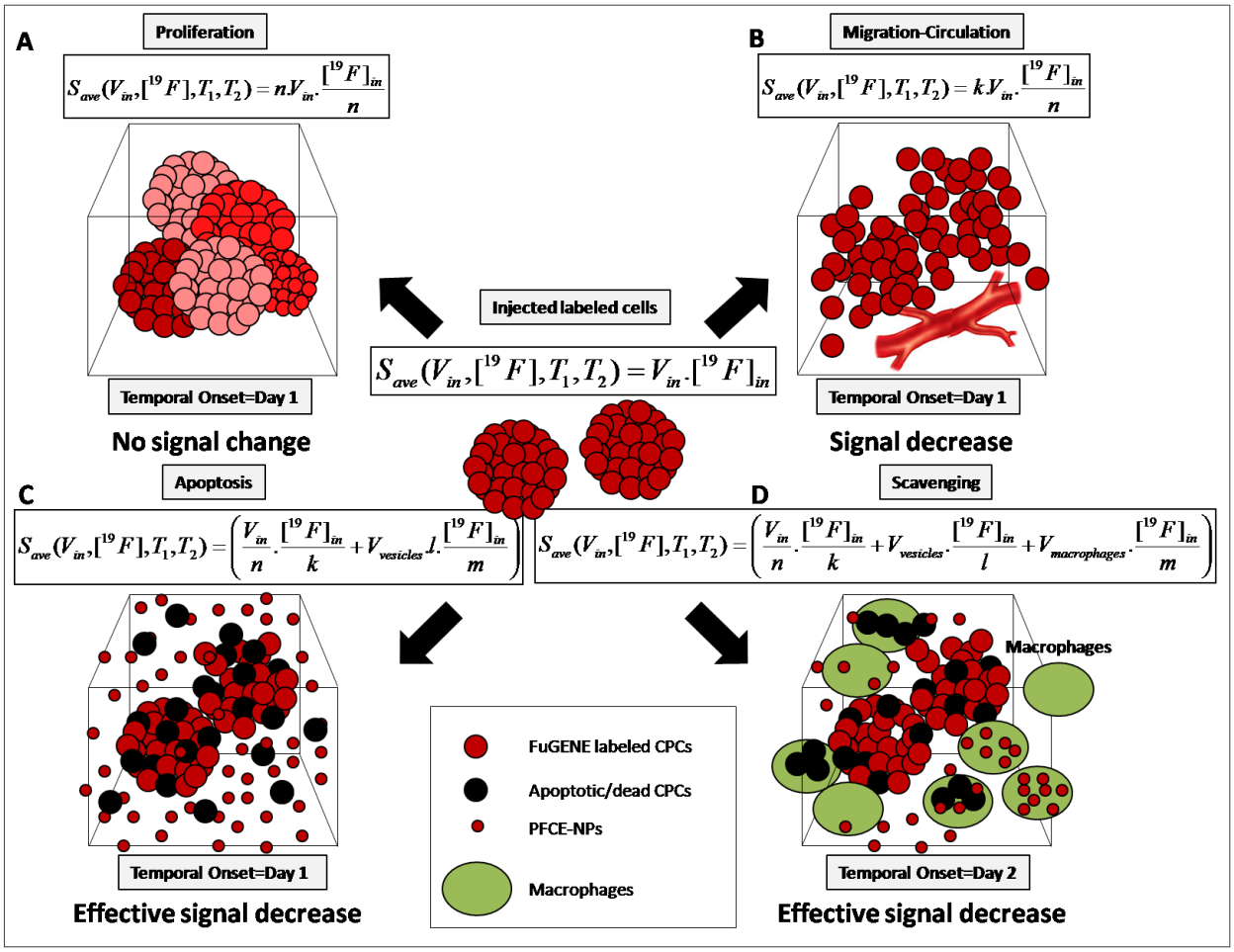

Figure 7: Proposed models of temporally dependent ^{19}F decreases in tracking studies. Schematics represent typical image voxels containing injected, labeled CPCs, apoptotic CPCs, macrophages, and PFCE-NPs, and the prominent mechanisms that may affect voxel-volume averaged signal intensity, as these modulate intracellular/extracellular volume and fluorine content. Possible relaxation changes (T_1, T_2) are ignored. Symbols S_{ave} denote average signal intensities, V volumes (intracellular, vesicular, macrophage), and [^{19}F] fluorine concentrations. Indices k, l, m, and n, denote symbols for real numbers that quantify intracellular volume or fluorine changes within the voxel.

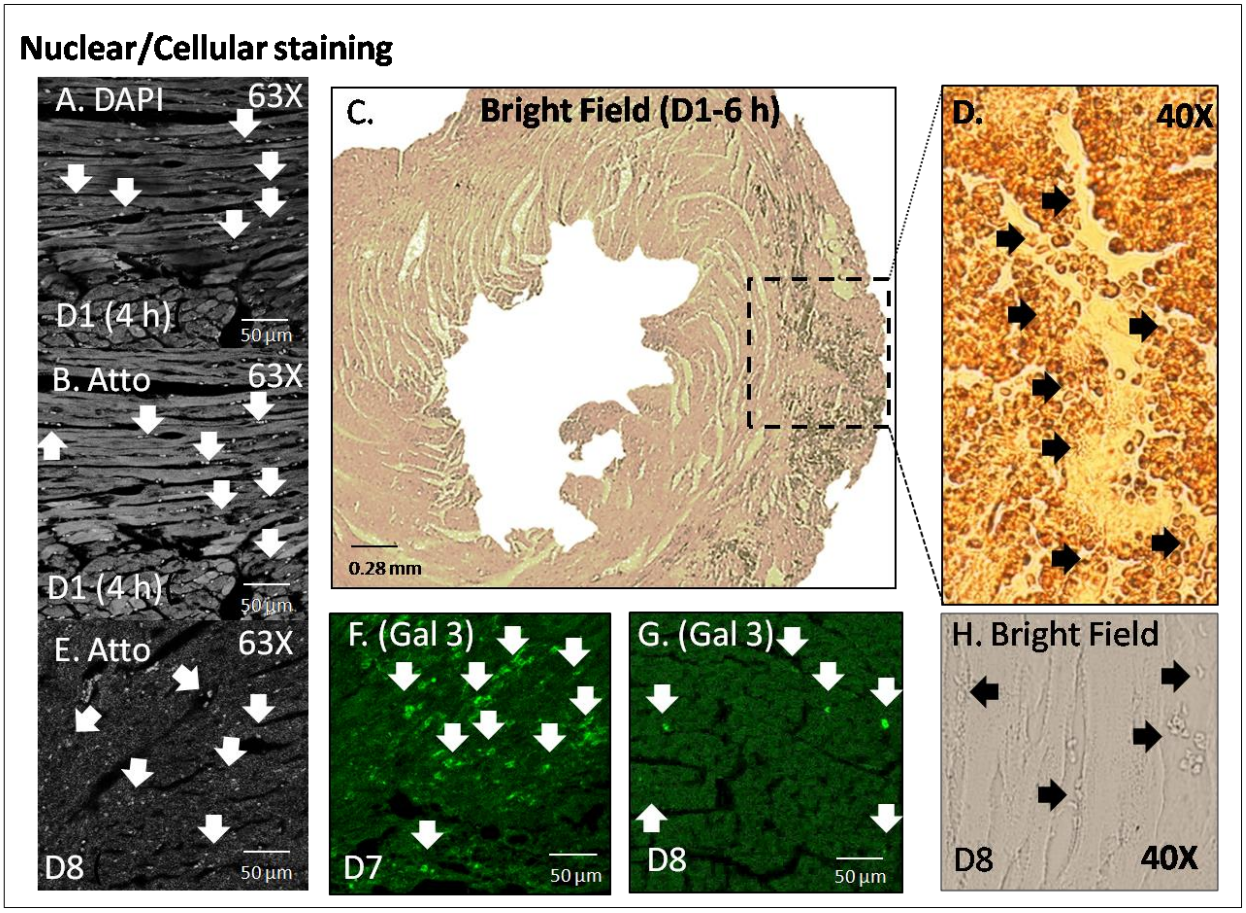

Figure 8: Nuclear, bright field histological and immunostaining imaging. (A–E) Histological unstained and stained sections of murine hearts in justification of the retention of injected labeled cells, based on nuclear (DAPI), and surface marker (Atto647) staining (bright spots) using confocal imaging. (C) Histological/stained short-axis, mid-apical views of three murine hearts ([A–D] terminal experiments in two mice at (A, B) 4 and (C, D) 6 h post-cell injection on day 1 (D1), and [E–H] on D7/D8) indicating the sites of injected CPCs using bright field (C, D, E, H), nuclear (A), surface (B, E, Atto647), and immunostaining (F-G, Galectin3 (Gal3)), using confocal imaging.

Supplementary Material

Cell Isolation and Labeling

Cell Isolation: Cardiac progenitor cells (CPCs) were isolated from adult, C57BL/6, or C57BL/6-Tg(CAG-EGFP)1Osb/J (The Jackson Laboratory, Bar Harbor, ME, USA) mouse atria. Cardiosphere-derived cells (CDCs) were expanded as described previously [1]. Collagenase/Trypsin (CT) cells were isolated by digestion of atrial tissue with 0.05% trypsin-EDTA and adhered on fibronectin-coated petri dishes over periods of 72 h [2].

Labeling-Viability: Cells were plated in Iscove's Modified Dulbecco's Medium (IMDM, Thermo Fisher Scientific, UK) and incubated in culture with fluorescent PFCE-NPs (Atto647, ATTO-TEC, GmbH, Germany) (10 mg/million cells) [3], for ~24 h before trypsinization, isolation, and pelleting. Cell viability was assessed using the Trypan Blue exclusion assay.

FuGENE Optimization: FuGENE (Promega, Madison, WI, USA) was used to label the cells with the NPs. To optimize the dose, three different FuGENE doses were used in two separate experiments (25, 100, and 200 μl of FuGENE in ~10^6cells). FuGENE was pre-mixed and incubated with the NPs for ~20 min before cell labeling. Cells were transfected overnight.

Electroporation: Cells were resuspended in 400μl of IMDM media and were electroporated using a BIORAD Gene PulserX cell electroporator unit (BIORAD, Hertfordshire, UK) using a single rectangular pulse (amplitude 250 V, duration 5 ms). They were then resuspended in a larger volume of IMDM media for epifluorescence and MR imaging.

Labeling efficiency: Labeling efficiency was determined with a CyAn ADP flow cytometer (Beckman Coulter, Indianapolis, IN, USA). Processing was conducted offline using FlowJo (FlowJo LLC, Version 10, Ashland, OR, USA). Cells were determined to be positively labeled (with 95% confidence) by comparison to the fluorescence of unlabeled cell samples.

Cell Fixation: Cells destined for flow cytometry were fixed in a 2% methanol-free formaldehyde solution (Thermo Scientific Pierce, UK), mixed with phosphate buffer solution (PBS) (1:7 v/v) (Sigma-Aldrich, UK), in final solutions containing 0.5-1 ml.

Transverse Electron Microscopy: For transverse electron microscopy (TEM), pellets of cell extracts were blocked in agar, fixed in 2.5% glutaraldehyde, washed in 0.1 M phosphate buffer (Sigma-Aldrich, UK), fixed in 1% osmium tetroxide, dehydrated in increasing concentrations of ethanol, and embedded in an epon araldite/resin mixture. The resin was polymerized at 60 °C overnight and ultrathin sections were cut using a Reichert Jung ultramicrotome (Vienna, Austria) with thicknesses in the range of 80-100 nm. Sections were stained with lead citrate and uranyl acetate, before being examined with a JEM 1010 TEM operating at 80 kV (JEOL, Tokyo, Japan).

MRI/MRS

The 9.4T scanner was equipped with a Direct Drive console and a 1000 mT/m actively shielded gradient set (internal diameter=60 mm) (Agilent Technologies, Santa Clara, CA, USA).

Radiofrequency Coils: For MRI studies, a 4×4 cm^2 single-turn, transmit/receive butterfly (on a 28 mm diameter plastic former) and a custom-made solenoid coil, were used as described

previously [2, 4]. The broad frequency response of the coils allowed intermittent $^{1}H/^{19}F$ MRI/MRS. To minimize the B_1 effects, all samples used for in vitro and quantification studies were consistently placed on the coils.

^{19}F MRI-Phantom Studies: a) Aqueous cylindrical phantoms containing trifluoroacetic acid (TFA) (100 and 200mM) and NaF solutions (50–200 mM) [Sigma-Aldrich, UK] were used to optimize the radiofrequency (RF) coil response using the conventional spoiled gradient echo (SPGR) ^{19}F MRI sequences as reported previously [4].

Separate phantoms containing PFCE-NPs (8 mg/ml) sonicated in deionized water and mixed in cell media (IMDM, Thermo Fisher Scientific, UK) to an Eppendorf volume of 1.7 ml comprising a) separate TFA and FuGENE vials (200 μl), b) separate TFA, NPs, and FuGENE vials, and c) a separate TFA and a pre-mixed NP/FuGENE vial (200 μl), were used for control phantom validations using ^{19}F MRS (repetition time (TR)=20s, pw=32–80 μs, bandwidth (BW)=19.84 kHz, number of excitations (NEX)=16, 512–1024 points), using the solenoid coil [2].

The acquisition parameters for all other in vitro studies were: TR=5.71 ms, echo time (TE)=2.87 ms, flip angle=50°, NEX=256, matrix=32×32, dummy scans=100, slice thickness (ST)=15 mm, BW)=6.01 kHz, field-of-view (FOV)=40–60×40–60 mm^2. For MRS, fully relaxed spectra were acquired for cell studies.

In Vivo Cardiac ^{19}F MRI and Cellular Tracking

^{1}H Imaging: Double-gated, two-dimensional (2D) multislice, and ungated 2D/3D spoiled grass (SPGR) cardiac ^{1}H images (to match the corresponding ungated ^{19}F MRI) of the mouse thorax were acquired in vivo (2D: TR/TE=1.9–2.13/1–1.1 ms, flip angle=20–50°, NEX=2–6,

FOV=40×40 mm^2, matrix=128×128, acquisition time=3-5 min;3D: TR/TE=1.9–2.13/1–1.1 ms, flip angle=20–50°, NEX=2–6, FOV=40×40 mm^2, matrix=128×128×128, acquisition time=3–5 min).

^{19}F MRI/MRS: Ungated ^{19}F SPGR images matched ^{1}H MRI (2D: TR/TE=16.5/8.3 ms, flip angle=50°, NEX=768, FOV=40×40 mm^2, 1 slice, ST=5 mm, matrix=32×32, BW=2–4 kHz, acquisition time=2.42 min; 3D:TR/TE=16.4/8.3 ms, flip angle=20–30°, NEX=12–72, FOV=40×40 mm^2, matrix=32×32×32, BW=1–3 kHz, acquisition time=3–19 min**).** The excitation frequency for ^{19}F acquisitions was determined based on nonlocalized saturation recovery, gated ^{19}F MRS of the labeled CPCs acquired a priori (TR=800–1200 ms, 512 points, BW=20kHz, NEX=128–256).

Image Processing

Image and Spectral Analyses: ^{19}F images were imported and interpolated (bicubic splines) in ImageJ (NIH, Bethesda, MD, USA) to match the ^{1}H matrix size. Thoracic ^{1}H and ^{19}F MRI were overlaid in ImageJ (opacity=30–70%). SNR values were estimated using standard methodologies. For in vitro studies, fluorine concentrations were evaluated by estimating the areas of fully relaxed spectra with respect to a TFA reference standard of known concentration. For tracking studies, the mean signal was estimated as the average ^{19}F signal from all images in the 3D stack in ImageJ. Spectra were read and processed in CSX (P. Barker, Johns Hopkins, Baltimore, MD, USA) or using custom-written IDL tools (Harris Geospatial Solutions, Broomfield, CO, USA).

Epifluorescence Image Analyses: No localized fluorescence signals were detected from control (unlabeled) cells. The mean fluorescent intensities quantified in control studies were attributed to noise and auto-fluorescence and matched the mean signal intensities from labeled cells at D4-D7. Labeled cell detection (D1, D4, or D7) was based on fluorescence threshold intensity detection at values above the background intensity (as determined from background non-cellular regions at D1, D4, or D7).

References (Supplementary Material)

1. Perbellini F, Gomes RS, Vieira S, Buchanan D, Malandraki-Miller S, Bruyneel AA, et al. Chronic high-fat feeding affects the mesenchymal cell population expanded from adipose tissue but not cardiac atria. Stem Cells Translational Medicine 2015; **4(12)**:1403–14. DOI: 10.5966/sctm.2015-0024.

2. Constantinides C, McNeill E, Benson M, Urruela RS, Padilla S, Malandraki-Miller S, et al. Improvements in the cellular uptake of perfluorocarbon nanoparticles and ^{19}F MRS/MRI detectability using the transfection agent FuGENE. ISMRM Workshop on Molecular and Cellular MRI: Focus on Integration: Amsterdam, Netherlands, June 2016.

3. Srinivas M, Cruz LJ, Boneto F, Heerschap A, Figdor CG, de Vries IJM. Customizable, multi-functional fluorocarbon nanoparticles for quantitative in vivo imaging using ^{19}F MRI and optical imaging. Biomaterials 2010; **31**:7070–7077.

4. S. Malandraki-Miller, R. Tyser, P. Riley P, C.A. Carr. Comparative characterization of cardiac atrial progenitor cell populations for use in cell therapy, Heart **100** (2014) A14.

Supplementary Figure Captions

Supplementary Figure S1: Temporally dependent cellular responses following labeling and FuGENE labeling. Transverse electron microscopy (TEM) images from control, labeled, and FuGENE-labeled cells. (A-C) Typical EM images from control CT cells harvested on D1 after plating. Sequence of EM images (D1-D3) following (D-F) labeling and (G-I) FuGENE-labeling.

Supplementary Figure S2: Study of the temporal label kinetics using dynamic confocal imaging. Study of the temporal label kinetics using dynamic confocal imaging (labeling [**Movie 1**: acquired at 1.2 h post-label administration], optimal [**Movie 2**: 25 μl per million cells acquired at 5.7 h post-label administration], and high FuGENE doses [**Movie 3**: 100 μl per million cells acquired at 4.15 h post-label administration]) confirming increased (Movie 2), decreased (Movie 1) intracellular label uptake and cluster formations (Movie 3) at high FuGENE doses. Significant label uptake was confirmed within 2-3 h post-label administration. Label uptake was distinguished from transient particle adherence on the extracellular membrane based on 3D visualizations and cross-correlations of single-cell phase contrast and confocal images post-labeling. Indicative 2D examples are depicted in Figure 4.

Supplementary Figure S3: Control validation experiments using MRS. (A-D) Control MRS experiment confirming that the source of ^{19}F signal is attributed to FuGENE-labeled NPs. In sequence shown are magnitude spectra (drawn to the same scale) of (A) TFA, (B) TFA and FuGENE (separate vials), (C) TFA, FuGENE and NP solution (separate vials), and (D) a real spectrum of TFA and FuGENE-NPs (mixed, same vial) (birdcage coil).

Supplementary Figure S4: FUGENE-labeling and electroporation studies with CDCs using MRS. (A-D) Pairwise comparisons (A and B, and C and D, drawn to the same scale) of nonlocalized, fully relaxed ^{19}F MRS responses of electroporated-labeled and FuGENE-labeled, and FuGENE-labeled and electroporated-FuGENE labeled CT cells (butterfly coil). Pairwise comparisons were conducted on separate occasions using single, separate samples in Eppendorf vials positioned at the same location on the butterfly coil.

Supplementary Figures

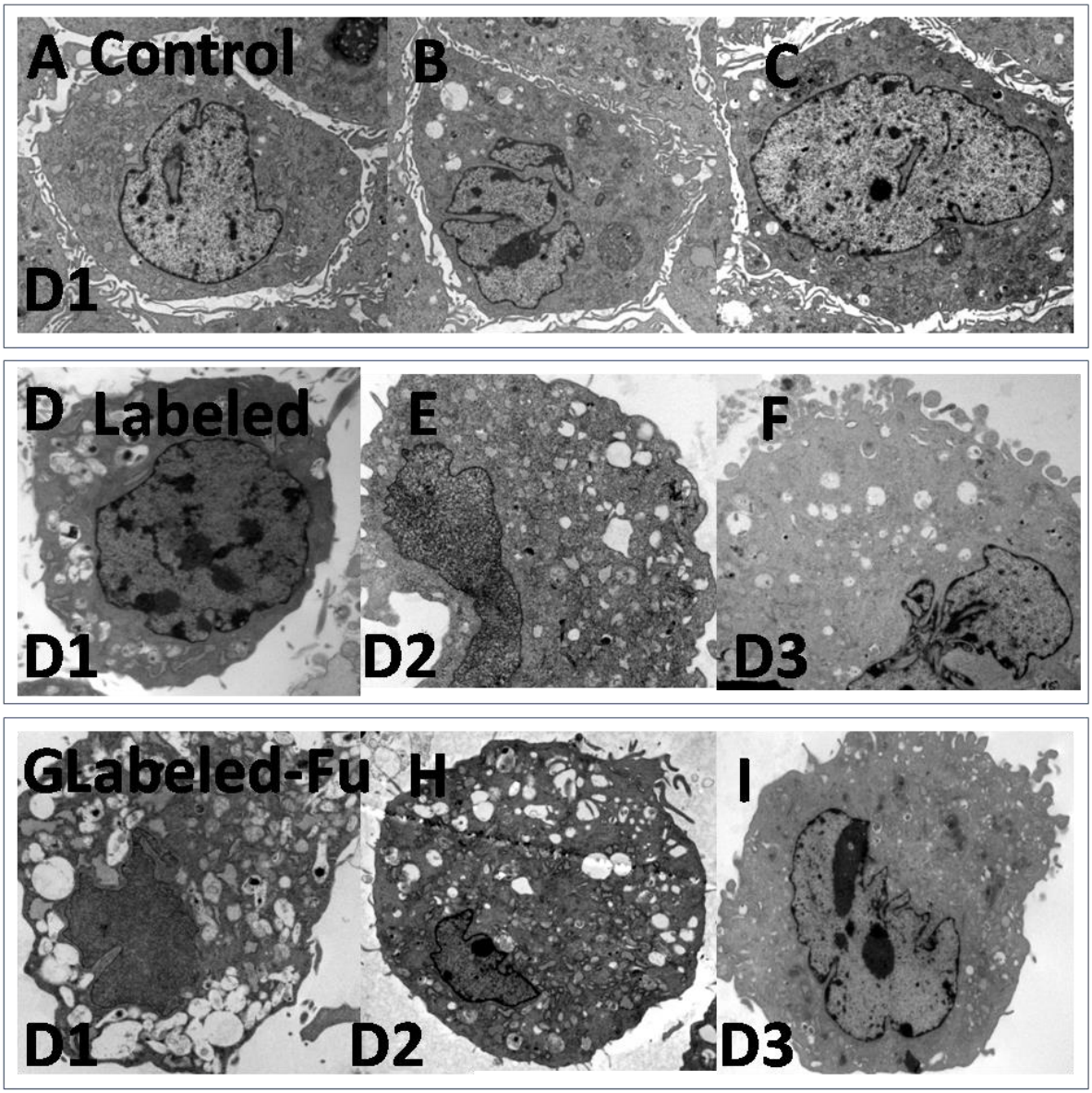

Supplementary Figure S1: Temporally dependent cellular responses following labeling and FuGENE labeling. Transverse electron microscopy (TEM) images from control, labeled, and FuGENE-labeled cells. (A-C) Typical EM images from control CT cells harvested on D1 after plating. Sequence of EM images (D1-D3) following (D-F) labeling and (G-I) FuGENE-labeling.

Supplementary Figure S2: Study of the temporal label kinetics using dynamic confocal imaging. Labeling [**Movie 1**: acquired at 1.2 h post-label administration], optimal [**Movie 2**: 25 µl per million cells acquired at 5.7 h post-label administration] and high FuGENE doses [**Movie 3**: 100 µl per million cells acquired at 4.15 h post-label administration]) confirming increased (Movie 2), decreased (Movie 1) intracellular label uptake and cluster formations (Movie 3) at high FuGENE doses. Significant label uptake was confirmed within 2-3 h post-label administration. Label uptake was distinguished from transient particle adherence on the extracellular membrane based on 3D visualizations and cross-correlations of single-cell phase contrast and confocal images post-labeling. Indicative 2D examples are depicted in Figure 4.

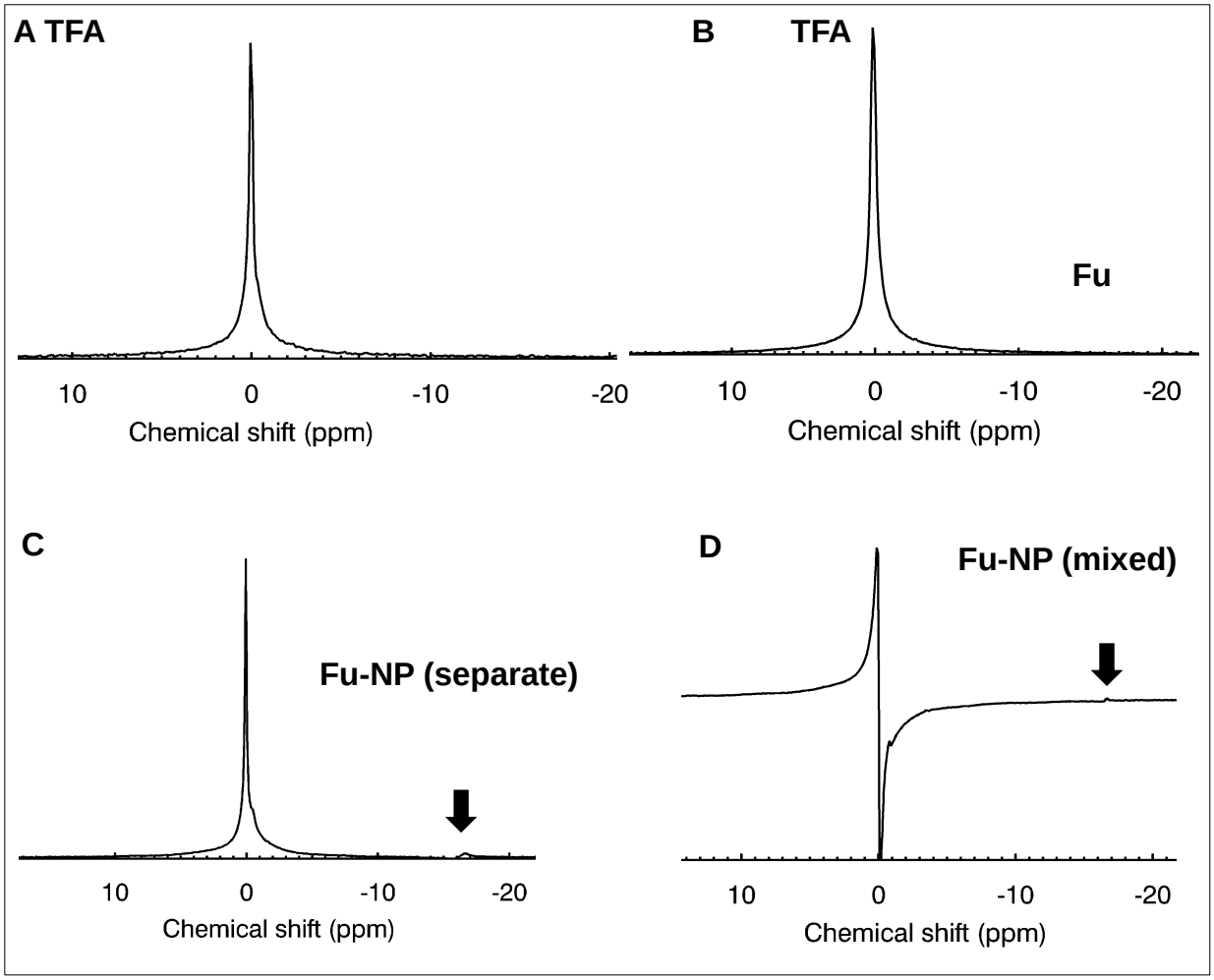

Supplementary Figure S3: Control validation experiments using MRS. (A-D) Control MRS experiment confirming that the source of ^{19}F signal is attributed to FuGENE-labeled NPs. In sequence shown are magnitude spectra (drawn to the same scale) of (A) TFA, (B) TFA and FuGENE (separate vials), (C) TFA, FuGENE and NP solution (separate vials), and (D) a real spectrum of TFA and FuGENE-NPs (mixed, same vial) (birdcage coil).

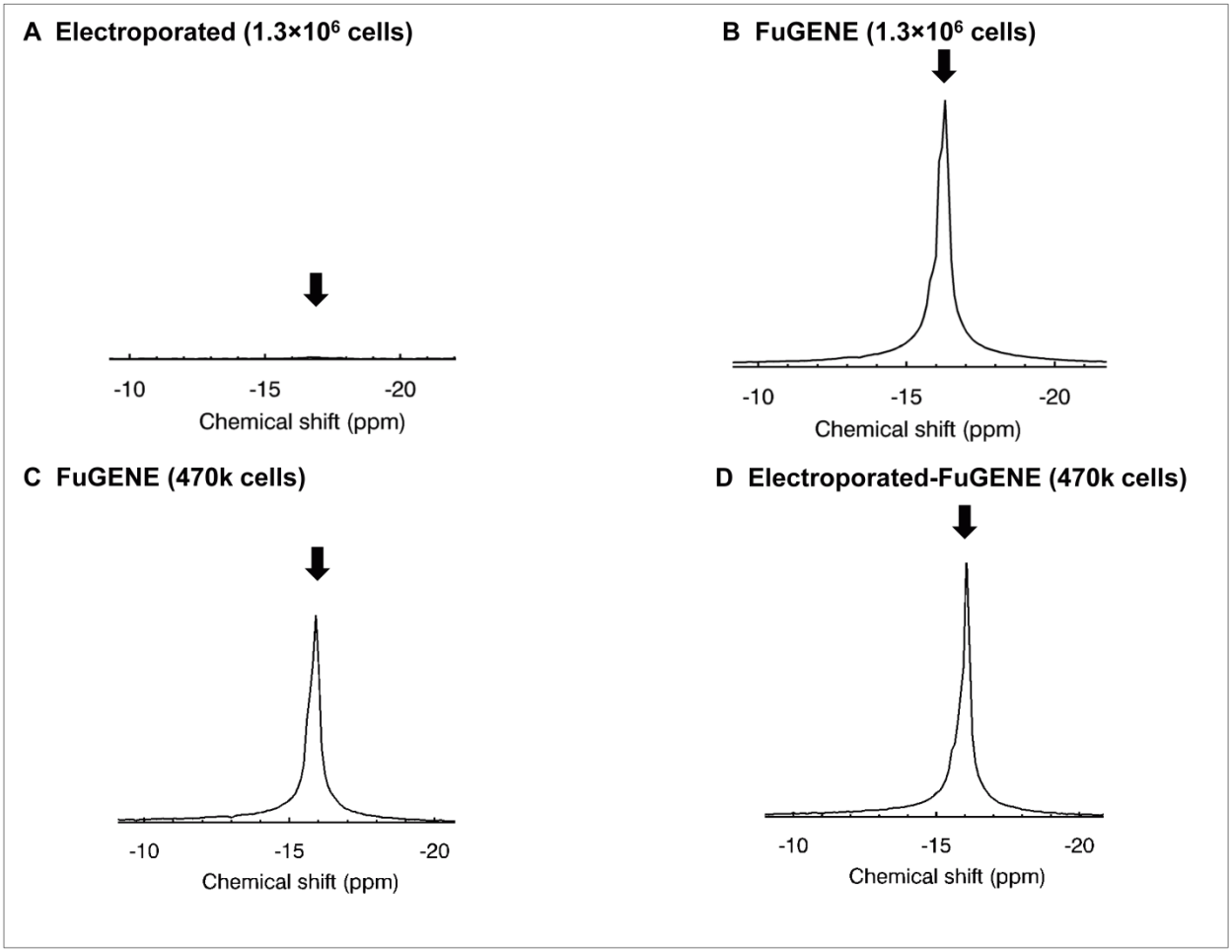

Supplementary Figure S4: FUGENE-labeling and electroporation studies with CDCs using MRS. (A-D) Pairwise comparisons (A and B, and C and D, drawn to the same scale) of nonlocalized, fully relaxed ^{19}F MRS responses of electroporated-labeled and FuGENE-labeled, and FuGENE-labeled and electroporated-FuGENE labeled CT cells (butterfly coil). Pairwise comparisons were conducted on separate occasions using single, separate samples in Eppendorf vials positioned at the same location on the butterfly coil.